ACS APPLIED MATERIALS & INTERFACES

Research Article

www.acsami.org

Lightweight Polypropylene/Stainless-Steel Fiber Composite Foams with Low Percolation for Efficient Electromagnetic Interference Shielding

Aboutaleb Ameli, Mohammadreza Nofar, Sai Wang, and Chul B. Park*

Microcellular Plastics Manufacturing Laboratory, Department of Mechanical and Industrial Engineering, University of Toronto, 5 King's College Road, Toronto, Ontario Canada M5S 3G8

ABSTRACT: Lightweight polypropylene/stainless-steel fiber (PP−SSF) composites with 15−35% density reduction were fabricated using foam injection molding. The electrical percolation threshold, through-plane electrical conductivity, and electromagnetic interference (EMI) shielding effectiveness (SE) of the PP−SSF composite foams were characterized and compared against the solid counterparts. With 3 wt % CO_2 dissolved in PP as a temporary plasticizer and lubricant, the fiber breakage was significantly decreased during injection molding, and well-dispersed fibers with unprecedentedly large aspect ratios of over 100 were achieved. The percolation threshold was dramatically decreased from 0.85 to 0.21 vol %, accounting for 75% reduction, which is highly superior, compared to 28% reduction of the previous PP−carbon fiber composite foam.[1] Unlike the case of carbon fiber,[1] SSFs were much longer than the cell size, and the percolation threshold reduction of PP−SSF composite foams was thus primarily governed by the decreased fiber breakage instead of fiber orientation. The specific EMI SE was also significantly enhanced. A maximum specific EMI SE of 75 $dB{\cdot}g^{-1}{\cdot}cm^3$ was achieved in PP−1.1 vol % SSF composite foams, which was much higher than that of the solid counterpart. Also, the relationships between the microstructure and properties were discussed. The mechanism of EMI shielding enhancement was also studied.

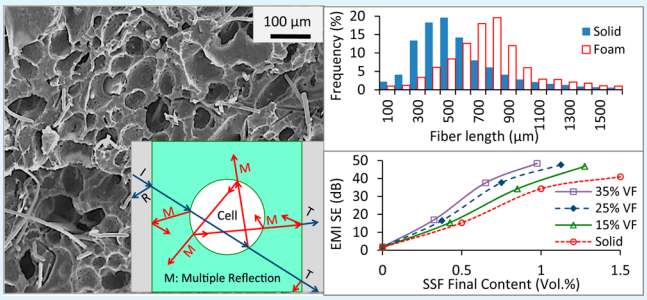

KEYWORDS: *electrical properties, electromagnetic interference shielding, percolation, foam, polymer−matrix composites*

1. INTRODUCTION

With the rapidly increasing usage of electronic and microelectronic devices, the unintentional generation, propagation, and reception of electromagnetic energy are becoming one of the major concerns. Such devices radiate and are affected by electromagnetic interference (EMI). Proper EMI protection is thus an essential requirement to ensure their continued functionality and integrity, to control their EMI emission level as required by the standards imposed by governmental agencies,[2] and to minimize their radiative damage to the human body.[3] Metal-based shields and conductive coatings are the most widely used EMI protectors.[4] However, metallic shields have some drawbacks such as high density, corrosion, and expensive processing. Metallic coatings also require an extra step of processing and experience delamination issues.[4]

Conductive polymer composites (CPCs) are becoming promising candidates to be employed as EMI shields because they offer light weight, low cost, high processing ability, and high resistance to corrosion, and various CPCs containing conductive microsized[5−10] or nanosized[11−16] fillers have been developed for EMI shielding applications. However, CPCs are not yet very successful in replacing the metal-based shields because of the high filler loading that is required to achieve a sufficient level of shielding. This adversely affects the processability, weight, and economic feasibility of the product. Particularly, the weight reduction of CPCs is desirable in numerous applications such as the aerospace and automotive industries.

Furthermore, CPCs are usually processed using injection molding as one of the cost-effective manufacturing methods. However, the nature of the injection-molding process introduces further challenges because it results in (a) a significant reduction of the filler aspect ratio due to fiber breakage,[1,17,18] (b) anisotropic electrical conductivity due to the in-plane and/or longitudinal orientation of fibers,[1,19] and (c) higher percolation thresholds.[18]

Foaming may provide a sustainable route to address some of the CPC shortcomings by decreasing the density, easing the processing, and improving the performance.[17−24] First, the blowing agent dissolved in the matrix decreases the composite viscosity by the plasticizing effect of gas (i.e., increased molecular mobility) and eases the processing.[17,20] Second, the presence of gas will effectively decrease fiber breakage and yield a larger aspect ratio,[1,17] and thus a lower percolation threshold. Foaming can also effectively disturb the in-plane orientation of the fiber, decrease the size of the skin layer that has highly

Received: January 21, 2014
Accepted: June 25, 2014
Published: June 25, 2014

oriented fibers, and thus enhance the through-plane conductivity.[19,20,23] Moreover, the dissolved gas can also prevent fiber aggregation and improve the dispersion[23,24] and distribution[19,20] of the fibers, which is helpful in lowering the electrical percolation threshold.[25,26] It has also been shown that a conductive filler acts as heterogeneous cell nucleating agent, which can increase the cell nucleating power of composites.[27] Therefore, the generation of a cellular structure into conductive composites by physical foaming can contribute to the reduction of density, increase of processability, and enhancement of the performance. It is noted that foam injection molding creates some through-plane density and cellular morphology gradients. However, the effects of such gradients on the electrical conductivity and EMI SE will be marginal in the case that the fiber length is significantly greater than the cell size because the fiber orientation will not be significantly affected by cell growth.

Recently, some researchers have tried to develop CPC foams for EMI shielding applications.[1,13,28−40] Thomassin et al.[31] used melt-blending and coprecipitation techniques to prepare polycaprolactone (PCL)/multiwalled carbon nannotubes (MWCNT) composite foams with densities as low as 0.22 g·cm^{-3} and EMI shielding effectiveness (SE) of as high as 80 dB at MWCNT loading of 0.1−0.54 vol % and a shield thickness of 20 mm. Ling et al.[28] reported microcellular poly(ether imide) (PEI)/10 wt % graphene nanocomposite foams, prepared by a phase-separation process, that exhibit a density of ∼0.3 g·cm^{-3} and a specific EMI SE of 44.1 dB·g^{-1}·cm^3. Yan et al.[35] also used a salt-leaching process to prepare polystyrene (PS)/30 wt % graphene foams and achieved a SE of 29 dB, corresponding to a specific SE of 64.4 dB·g^{-1}·cm^3. Recently, Chen et al.[36,37] used a nickel template to deposit graphene sheets by chemical vapor deposition. After the graphene layer was coated with poly(dimethylsiloxane) (PDMS) and the nickel template was etched, highly flexible foams of low density (0.06 g·cm^{-3}) were obtained and presented a high specific EMI SE of 500 dB·g^{-1}·cm^3.[36]

However, most of these efforts have been focused on batch-scale systems that cannot be easily scaled up, and very little attention has been paid to the foam injection-molding process of CPCs for EMI shielding applications. One major advantage of foam injection molding is that it can be easily adapted to manufacture EMI shields as substitutes for metal-coated thermoplastic frames and cabinets because they are currently manufactured by injection molding. In our earlier works, the effects of foaming (using nitrogen, cell size ≈ 100 μm) and injection-molding parameters on the microstructure, the electrical properties, and the EMI SE of injection-molded polypropylene (PP)−carbon fiber (∼100 μm length and stiff) composites were investigated.[1,20] It was shown that generation of a cellular structure reduced the density of the injection-molded samples by 25%, lowered the volume fraction of the percolation threshold from 8.5 to 7 vol %, enhanced the through-plane conductivity, increased the dielectric permittivity, and resulted in an increase of the specific EMI SE up to 65%.[1,20]

In this work, stainless-steel fiber (SSF) was selected as a conductive filler to assess the effects of foaming in the injection-molding process when the fiber is flexible and its length is significantly larger than that of the cell size by an order of magnitude. Previous works dealt with the same size scale[1,20] or much smaller scale fibers[41] compared to the cell size. Unlike the previous cases,[1,20,41] in the current structural configuration, the change of the fiber orientation via cell growth is minimal, and thus the other mechanisms associated with physical foaming, particularly fiber breakage, were thoroughly investigated.

Also, carbon dioxide (CO_2) was selected as a physical blowing to have a much greater amount of dissolved gas in the polymer (3 wt %), as opposed to the case of nitrogen (0.3 wt %[1]). This is possible because of the higher solubility of CO_2, compared to that of nitrogen.[42,43] The higher gas content will contribute to a further decrease in the viscosity and thereby less fiber breakage and less fiber orientation. PP−SSF composites containing various fiber contents (0−1.5 vol %) were then made using injection molding to obtain solid and foam composites, having 0−35% void fraction. The effects of the introduction of a plasticizing gas and the void fraction on the electrical percolation threshold, the through-plane conductivity, and the EMI SE were characterized. The microstructure and fiber breakage were also investigated, and the mechanisms, through which foaming contributed to the enhancement of the electrical properties and the EMI SE, were also identified.

2. EXPERIMENTAL SECTION

2.1. Materials. The commercially available high-crystallinity injection-molding grade of homopolymer polypropylene (PP) F350HC2, with a specific gravity of 0.9 g·cm^{-3} and a melt flow index of 35 dg·min^{-1} (230 °C/2.16 kg), supplied by Braskem America Inc. (Houston, TX), was used as the base resin. Stainless-steel fiber (SSF), a grade of Beki-Shield GR75-C12-E supplied by Bekaert Corp. (Marietta, GA), was selected as the conductive filler. It was provided in the form of fiber bundles coated with ethylene acrylic acid zinc ionomer and sized with a thermoplastic polyester to yield 75 wt % of SSFs in the bundles. This grade was specifically designed to be used with polyolefins such as PP and in a processing temperature range of 120−290 °C. The SSFs had a length of 5 mm, an average diameter of 8 μm, and a specific gravity of ∼8 g·cm^{-3}. Commercial carbon dioxide (CO_2), supplied by Linde Gas, Canada, was used as the physical blowing agent for foaming.

2.2. Experimental Setup. A 50-ton Arburg Allrounder 270/320 C injection-molding machine (Lossburg, Germany) with a 30-mm-diameter screw and equipped with MuCell technology (Trexel, Inc., Woburn, MA) was used to fabricate solid and foam PP−SSF composites. The PP pellets and SSF bundles were directly fed into the injection barrel, and mixing occurred during processing. The SSF fibers were observed to be well distributed owing to the specific coating on the fibers and the dissolved gas. The mold contained a rectangular cavity with a fan gate of 1.5 mm gap after the sprue. The cavity dimensions were 132 mm × 108 mm × 3.2 mm. More details can be found in previous works.[44,45] The nominal void fraction in the foam samples was controlled using partial filling of the cavity.[46,47] The optimum processing parameters were selected based on their effects on the microstructure and electrical properties[20] and are listed in Table 1.

2.3. Microstructure. The microstructures were cryofractured, sputter-coated, and then examined using scanning electron microscopy (SEM; JEOL JSM-6060). The densities of the solid (ρ_s) and foam (ρ_f) composites were measured using the water-displacement method (ASTM D792-00). The void fraction was calculated as $(1 - \rho_f/\rho_s)$. To measure the fiber length, SSFs were first extracted from the polymer matrix by burning the composites at 400 °C for 1 h in a furnace. SSFs were then spread over a double-sided foam adhesive. The digital images of SSFs were then captured using optical microscopy, and image processing was carried out using *ImageJ* software, National Institutes of Health.

2.4. Electrical Conductivity. Disk-shaped samples of 20 mm diameter and 3.2 mm thickness were cut from the middle location of the injection-molded parts using a die cutter under compression molding. An Alpha-A high-performance conductivity analyzer by Novocontrol Technologies GmbH & Co. KG was used to measure the

Table 1. Processing Parameters Used in the Injection Molding of Solid and Foam Composites

parameter	solid	foam
melt temperature (°C)	220	220
barrel pressure (MPa)	18	18
screw speed (rpm)	450	450
metering time (s)	13	13
injection flow rate ($cm^3 \cdot s^{-1}$)	40	40
mold temperature (°C)	30	30
pack/hold pressure (MPa)	30	N/A[a]
pack/hold time (s)	3	N/A
gas injection pressure (MPa)	N/A	24
CO_2 content (wt %)	N/A	3
void fraction (%)	N/A	15, 25, 35

[a]N/A = not applicable.

through-plane electrical conductivity at a frequency range of 1×10^{-1}–3×10^{5} Hz. For comparison purposes, the direct-current conductivity, σ_{dc}, was taken at a frequency of 1×10^{-1} Hz. At least four sample replications were carried out for each case, and the average values were reported. In all cases, a voltage of 1.0 V was applied.

2.5. EMI Shielding. EMI SE was measured in the X-band frequency range (8.0–12.4 GHz) using the setup schematically shown in Figure 1. The setup consists of an HPE8361A programmable

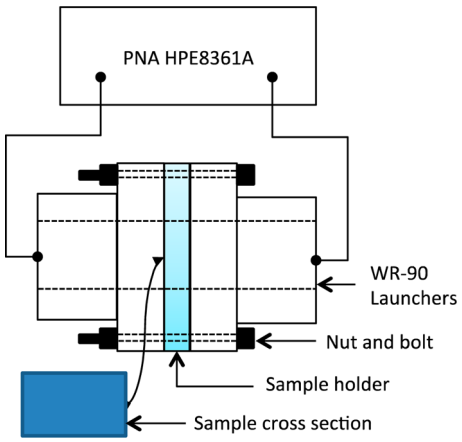

Figure 1. Schematic of the EMI SE measurement setup.

network analyzer (PNA), two standard WR-90 coaxial launchers to guide the electromagnetic wave, and a copper sample holder between the launchers. The sample was cut from the injection-molded parts and sized to 25 mm × 12.5 mm to fit in the opening of the sample holder, which had slightly bigger dimensions than the opening of the waveguide launchers (22.5 mm × 10 mm). The sample holder was then mounted between the launchers. The incident electromagnetic wave had a power of 0 dB·m, which corresponds to 1 mW. After calibration of the setup, the wave transmittance and reflectance were directly measured by the PNA and used to calculate the total EMI SE and its reflection and absorption components.[1]

3. RESULTS AND DISCUSSION

3.1. Electrical Conductivity. *3.1.1. Solid and Foam Injection-Molded Composites.* Figure 2 exhibits the electrical conductivity versus SSF content for the solid injection-molded (SIM) and foam injection-molded (FIM) PP–SSF composites. According to the percolation theory power law, the percolation threshold was found to be 0.85 vol % for SIM composites. The percolation threshold was calculated by fitting the experimental data in double-logarithmic scale to $\sigma = \sigma_0 (\varphi - \varphi_c)^t$, where σ

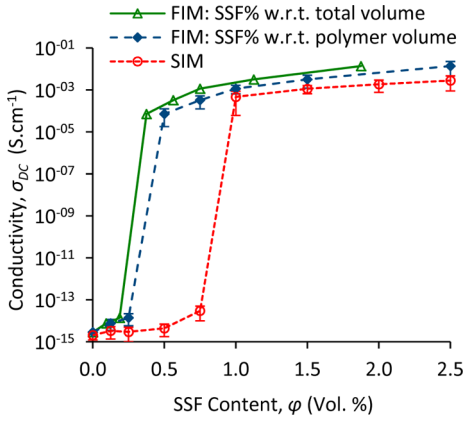

Figure 2. Electrical conductivity of SIM and FIM PP–SSF composites as a function of the SSF content. The foam samples have 25% void fraction.

and σ_0 are the measured conductivity and a scaling factor related to the filler intrinsic conductivity, respectively.[48] φ is the filler volume content, φ_c is the filler electrical percolation threshold, and t is a critical exponent related to the filler dispersion and dimensionality. It is notable that the percolation threshold of SIM composites is known to be much higher than that of solid compression-molded samples.[18,19,49,50] It is also reported that the through-plane conductivity of SIM samples beyond the percolation threshold is lower than that of the solid compression-molded samples at the same SSF content.[18,19,49,50] The reason for these differences stems from the difference in the state of orientation in injection- and compression-molded samples. Preferential orientation of the fibers in the flow direction is much more severe in the injection-molded samples compared to the compression-molded ones because of significantly higher shear forces applied to fibers in injection molding.[19,20]

It is also worth noting that the percolation threshold of SIM PP–SSF composites (0.85 vol %) was significantly lower than that of SIM PP–carbon fiber composites (~8.5 vol %) reported in our earlier work.[1] The major reason for such a low threshold in PP–SSF samples was the SSF's high aspect ratio. The fiber length measurement of SIM PP–1 vol % SSF showed that the fiber length had a number average of 570 μm, resulting in an aspect ratio of ~70, whereas that of the PP–carbon fiber was about 10.[1] In addition to the decreased percolation threshold, this range of fiber length provided the feasibility of investigating the foaming effect on the electrical conductivity when the fiber length is significantly greater than the cell size. This is important because the relative fiber size with respect to the average cell size would play a role in determining the degree of fiber orientation caused by cell growth.

The percolation graphs of FIM composites are also presented in Figure 2. They were analyzed in two different ways. Once, the SSF content was considered as the initial content in the solid precursor, taking only the polymer volume into account. However, after foaming, the gaseous volume was also introduced to the FIM samples. Therefore, to include the gaseous volume (i.e., the voids), the SSF content was also calculated with respect to the final volume of the injection-molded sample. Hereafter, these two SSF contents are called "initial" and "final", respectively. This type of analysis differentiated the effects of the foaming process and volume

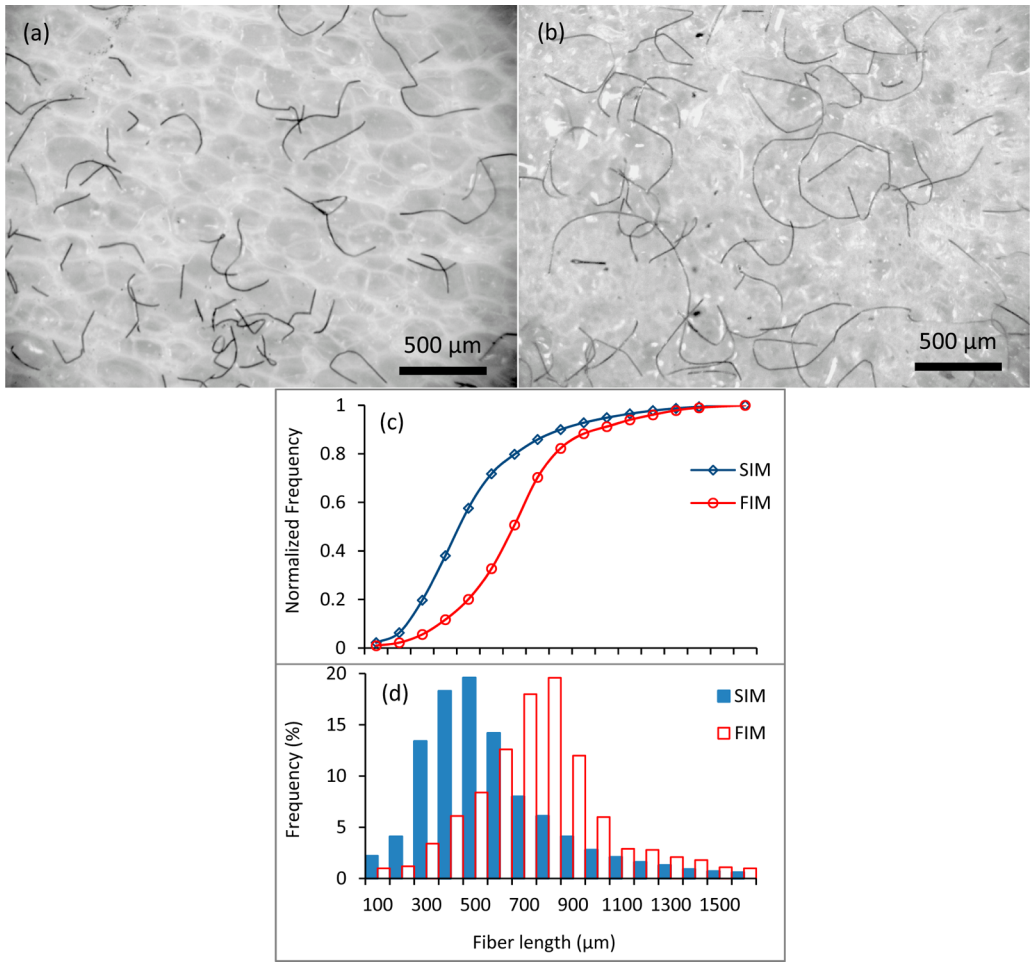

Figure 3. Representative optical micrographs of SSFs extracted from (a) SIM and (b) FIM composites and (c) cummulative and (d) frequency distribution of SSFs in PP−0.5 vol % SSF.

exclusion on the electrical conductivity of injection-molded samples.

The percolation threshold of the FIM samples was found to be 0.35 vol % based on the initial content (Figure 2). This is highly superior to 0.85 vol % in the SIM samples. Also, beyond the percolation threshold, foaming slightly increased the conductivity values of the injection-molded samples. Moreover, by taking the 25% void fraction into account, the percolation threshold further decreased from 0.35 to 0.26 vol %. In other words, the percolation threshold of injection-molded composites decreased by more than 3 times when a void fraction of 25% was generated in their structure.

The generation of foam may enhance the electrical conductivity of injection-molded samples via a change of the microstructure in several ways, i.e., by changing the degree of fiber breakage, fiber orientation, and skin layer thickness, as has been demonstrated before.[1,19,20] Figure 3 shows the representative optical micrographs and the fiber length distribution of both SIM and FIM PP−0.5 vol % SSF composites. Overall, the fiber length was higher in the FIM samples compared to that of the SIM samples. A number-average fiber length of 570 μm was obtained in SIM samples. However, the introduction of gas (3 wt % CO_2) into the polymer during processing resulted in less fiber breakage, and a number-average fiber length of 760 μm was achieved in FIM composites. Similar results have been observed for other fillers. Zhang and Thomson[17] and Ameli et al.[1] have shown that the degree of fiber breakage is decreased when foaming is employed in the injection molding of PP−glass fiber[17] and PP−carbon fiber composites.[1] Zhang and Thomson also measured the viscosity of PP−glass fiber using an in-line rheometer in the injection-molding process and found that the melt viscosity decreases in the presence of gas.[17] Therefore, the decreased viscosity decreased the shear stresses applied on the fibers and thus lowered the chance of fiber breakage. The larger preserved length of SSF in the FIM samples corresponded to an aspect ratio increase of more than 30%, compared to that in the SIM samples. It has been repeatedly reported that the percolation threshold decreases with an increase of the conductive filler aspect ratio.[1,51] Therefore, it can be concluded that the higher retained aspect ratio was another mechanism through which foaming enhanced the electrical conductivity of the injection-molded samples.

Foaming also contributed to the enhancement of the conductivity through changes in the state of fiber orientation. Figure 4 shows the representative microstructures of SIM and FIM PP−0.5 vol % SSF composites. In the SIM samples, the fibers tended to orient in the machine direction, with less tendency to orient in the thickness direction, as shown in Figure 4a. In the core and skin regions of the FIM samples, however, the fibers are oriented in both the machine and thickness directions (Figure 4b,c). The skin layer thickness was measured to be around 320 μm. This qualitatively indicates that

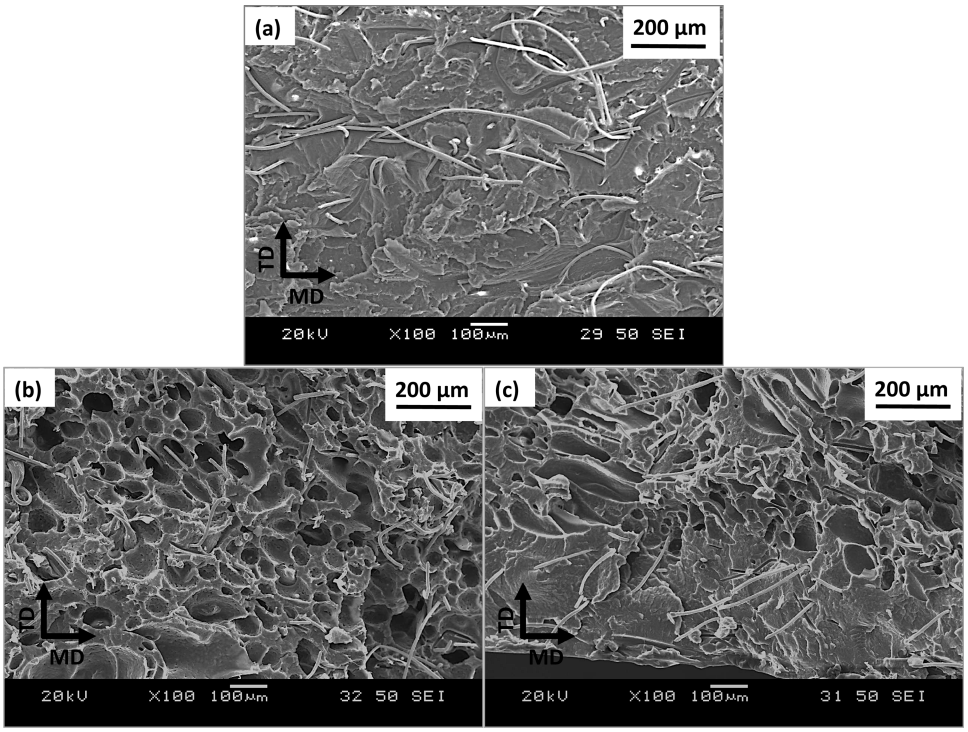

Figure 4. SEM micrographs of (a) SIM, (b) the core of FIM, and (c) the skin of FIM PP−0.5 vol % SSF composites. MD and TD denote the machine and thickness directions, respectively.

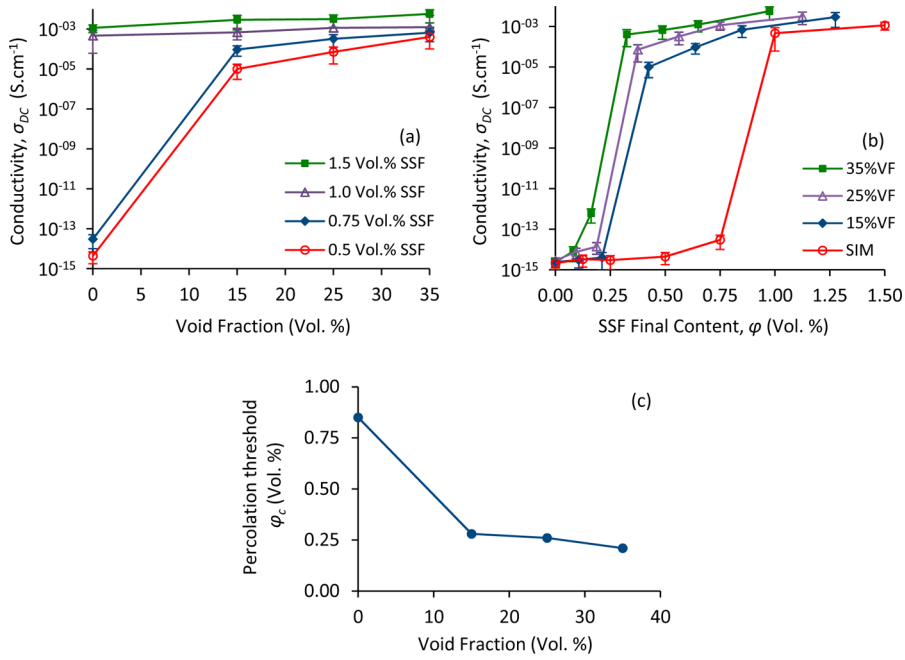

Figure 5. Effects of the void fraction on the electrical properties of PP−SSF composites: (a) variation of the conductivity with the void fraction in the composites containing various SSF initial contents; (b) evolution of the percolation graphs with the presence and an increase of the void fraction (0% void fraction denotes SIM samples): (c) reduction of the percolation threshold with the void fraction.

the severity of the preferential orientation was decreased because of the decreased viscosity in the presence of the dissolved gas.[1,19,20] The attenuation of this preferential orientation via the decreased viscosity by the presence of dissolved gas promoted the electrical conductivity in the thickness direction.[1,19,20]

It is notable that the foaming action in the core did not seem to affect the fibers' orientation much because of the smaller scale of cells compared to the fiber length. This is very different from the earlier cases, where the fiber size is equivalent to[1,20] or much smaller than[41] the cell size, where the foaming action affected the fiber orientation significantly. It is also believed that the skin layer thickness of the FIM samples was reduced with the presence of gas.[20] However, because of the difficulty in identifying the boundary of the skin layer for the unfoam SIM samples, this comparison was not possible.

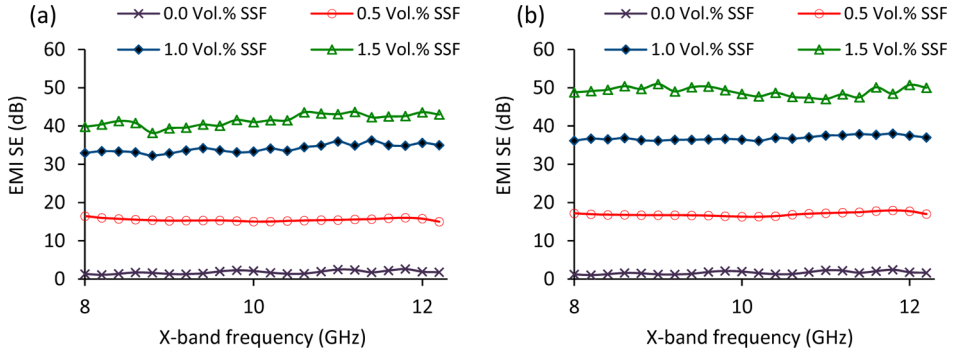

Figure 6. X-band frequency range of the EMI SE of (a) SIM and (b) FIM (25% void fraction) PP−SSF composites at various initial SSF contents.

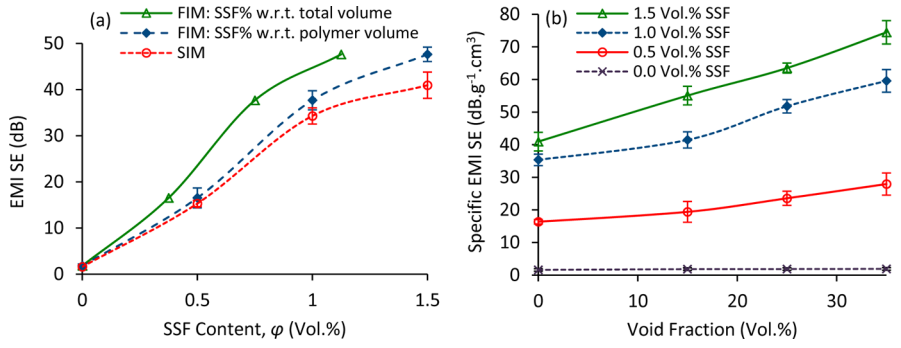

Figure 7. (a) EMI SE of SIM and FIM (25% void fraction) PP−SSF composites as a function of the initial and final SSF contents. (b) Specific EMI SE of PP−SSF composites as a function of the void fraction at various initial SSF contents.

3.1.2. Effect of the Void Fraction. Figure 5a exhibits the variations of the electrical conductivity with the void fraction for PP−SSF composites containing various initial SSF contents. Below the percolation threshold of the SIM samples (Figure 2), i.e., at 0.50 and 0.75 vol % initial SSF contents, the generation of 15% void fraction resulted in the formation of the percolative network and caused the insulation−conduction transition, and thus the electrical conductivity sharply increased by about 8−9 orders of magnitude. The electrical conductivity continued to gradually increase by a further increase of the void fraction from 15 to 35%. For instance, in PP−0.5 vol % SSF, the through-plane conductivity, σ_{dc}, increased from 4.3×10^{-15} to 4.0×10^{-4} S·cm^{-1} upon generation of 35% void fraction. At 1.0 and 1.5 vol % initial SSF contents above the percolation threshold, the conductivity increased very marginally with the void fraction. Because the percolation networks had already been formed in the solid samples at these contents, the conductivity enhancement was expected to be slight. In these composites, σ_{dc} increased 2−5 times after foaming.

To further investigate the effect of the void fraction on the electrical behavior, the percolation graphs of the PP−SSF composites having various void fractions are plotted in Figure 5b. Also, the percolation threshold was calculated for each void fraction using the percolation power law[48] $[\sigma = \sigma_0 (\varphi - \varphi_c)^t]$ and reported in Figure 5c. As seen, the percolation threshold, φ_c, decreased with an increase in the void fraction. First, φ_c sharply decreased from 0.85 to 0.28 vol % as 15% void fraction was generated. Then, φ_c slowly decreased from 0.28 to 0.21 vol % by a further increase in the void fraction to 35%. The sudden φ_c decrease at a 15% void fraction must be a coupled consequence of several factors: (a) the presence of dissolved gas in the polymer melt and its positive effects on the reduced viscocity, lessened fiber breakage, and attenuated preferential orientation of the fibers, (b) increased through-plane orientation of the fibers caused by the three-dimensional growth of cells,[1,19,20] and (c) volume exclusion by 15% gas phase. All of these factors contributed to the reduction of the percolation threshold when 15% foaming was generated. However, a further decrease of φ_c by an increase in the void fraction from 15% to 35% was mainly due to the increased polymer/fiber volume exclusion by the presence of higher gaseous volume, noting that the other aforementioned factors were relatively similar at various void fractions.

It is intersting to note that φ_c = 0.21 vol % for FIM PP−SSF composites with 35% void fraction accounts for more than a 4-fold decrease in the percolation threshold of the injection-molded samples. The φ_c = 0.21 vol % achieved here for the microsized SSF composites is significntly lower than the percolation threshold values reported for the solid composites containing microsized fillers such as carbon fiber (e.g., φ_c = 7.5 vol %[1] and φ_c = 1.5−4.5 vol %[52]), carbon black (e.g., φ_c = 2−6 vol %[53,54]), and SSF (e.g., $\varphi_c \approx$ 4 wt %[49]). In fact, φ_c values of FIM PP−SSF samples are comparable or even superior to those of the composites containing nanosized additives such as MWCNTs. For instance, percolation thresholds of 0.44 vol %,[54] 0.5 vol %,[55] ∼7 wt %,[56] and ∼3.5 vol %[57] have been reported for acrylonitrile butadiene styrene (ABS)−MWCNT, poly(methyl methacrylate) (PMMA)−MWCNT, polyethylene−MWCNT, and polyamide-6−MWCNT, respectively.

It is also noted that, in an our earlier work, an optimal void fraction of 20% was found for injection-molded PP composites containing short carbon fibers with an aspect ratio of ∼10.[20] However, for the current composites containing longer SSFs with an aspect ratio of ∼70, the conductivity was continuously improved with an increase in the void fraction of up to 35%. This trend suggests that a further increase of the void fraction

Table 2. EMI SE of Various Solid and Foam Materials Measured in the X-Band Frequency Range

	material	filler	thickness (mm)	EMI SE (dB)	specific EMI SE (dB·g^{-1}·cm^3)	specific EMI SE divided by thickness (dB·g^{-1}·cm^3·mm^{-1})
foam	PDMS−graphene[36]	0.8 wt %	1.0	20	333	333
	PS−graphene[35]	30 wt %	2.5	29	64.4	25.7
	PP−SSF (this work)	1.1 vol %	3.1	48	75	24.2
	PEI−graphene[28]	10 wt %	2.3	13	44	19.2
	PEI−graphene @Fe_3O_4[29]	10 wt %	2.5	17	42	16.8
	fluorocarbon−MWCNT[33]	12 wt %	3.8	42−48	50−57	13.2−15.0
	PP−carbon fiber[1]	10 vol %	3.1	25	34	10.9
	PCL−MWCNT[31]	2 wt %	20	60−80	193−258	9.7−12.9
	PMMA−graphene[30]	1.8 vol %	2.4	19	24	10.0
	PS−CNT[12]	7 wt %	N/A[a]	19	33	N/A
	PS−CNF[34]	15 wt %	N/A	19	N/A[a]	N/A
	poly(vinylidene fluoride)−graphene[32]	2 wt %	N/A	28	N/A	N/A
solid	poly(ether sulfone) (PES)−nickel filaments[59]	7 vol %	2.85	87	47	16.5
	copper[59]		3.1	90	10	3.2
	stainless steel[59]		4	89	11	2.7
	PES−nickel fibers[60]	10 vol %	3.1	7−13	N/A	N/A
	PS−copper nanowire[58]	2.1 vol %	0.21	35	N/A	N/A
	PES−carbon fiber[60]	40 vol %	2.87	30−38	N/A	N/A
	PES−nickel particles[61]	9.4 vol %	2.82	23	N/A	N/A

[a]N/A indicates that the value has not been reported.

beyond 35% may still contribute to the further enhancement of the conductivity and the percolation threshold of PP−SSF composite foams. In other words, the composites' density can be further decreased while the electrical performance is also enhanced. This is due to the fact that the fiber thinning via cell growth would not adversely affect the fiber interconnection. Because the fiber length is much greater than the cell size, cell growth would not be able to change the relative location of the fibers.

3.2. EMI SE. EMI SE is a measure of the material's ability to attenuate the electromagnetic wave intensity. For electromagnetic radiation, EMI SE is the logarithm of the ratio of incident power (P_i) to transmitted power (P_t) in decibels, i.e., SE = 10 log(P_i/P_t). For example, SE of 20 and 40 correspond to the blocking of 99% and 99.99% of electromagnetic incident waves, respectively. The EMI SE of the injection-molded PP−SSF composites was measured in the X-band frequency range (8.2−12.4 GHz) and is presented in Figure 6. As can be seen, both solid and foam composites exhibited relatively frequency-independent shielding behavior at various SSF contents and the SE increased as the SSF content increased.

The grand average values over the X-band frequency range are reported as representative SE in Figure 7. As can be seen, FIM samples (25% void fraction) presented higher SE values than their corresponding SIM composites with the same initial SSF content. At 1.5 vol % SSF, SE of the FIM samples reached 47.6 dB, while that of the SIM samples was 40.9 dB. This corresponded to an increase in SE of about 15%. Similar effects of foaming have been shown in carbon fiber composites.[20]

Figure 7a also depicts the EMI SE of FIM composites as a function of the SSF volume percent with respect to the total volume of the foam sample (i.e., final content). It is seen that the final SSF content required for the foam composites to achieve a certain level of SE is significantly lower than that in the solid composites. For instance, to achieve a SE of ∼40 dB, 1.5 vol % SSF is required for the SIM samples while only slightly more than 0.75 vol % SSF is sufficient if the composite has 25% void fraction. This accounts for ∼50% less usage of SSF when foaming was employed. Furthermore, in the FIM samples, only 0.37 vol % was enough to reach SE = 16.5 dB, which is in the range required for applications in computer devices.[58]

In the applications where lightweight materials are required, the density is as important as the SE value. Therefore, the specific EMI SE, defined as the ratio of the SE to the density, provides a more appropriate criterion to compare the EMI shielding performance. Figure 7b depicts the specific EMI SE of PP−SSF composites as a function of the void fraction. In all of the SSF contents, the specific EMI SE proportionally increased with the void fraction. A maximum specific SE of 75 dB·g^{-1}·cm^3 was achieved in the composites with 1.1 vol % final SSF content (i.e., 1.5 vol % in the solid precursor; Figure 7b) and 35% void fraction.

The specific EMI SE of 75 dB·g^{-1}·cm^3 is highly superior to the performance of most of the EMI shielding materials reported in the literature, as summarized in Table 2. Furthermore, the volume percentage of the filler used in the PP−SSF composite foams is lower than those reported in most of the works (Table 2). Because the SE is a strong function of the shield thickness and it is usually directly proportional with the thickness, to facilitate a more direct comparison, the specific EMI SE of various materials was divided by the thickness of the tested shield and presented in Table 2. It is seen that a value of 24.2 dB·g^{-1}·cm^3·mm^{-1} was obtained for the current work, which is superior to those of most of the reported works. A significantly higher value of 333 dB·g^{-1}·cm^3·mm^{-1} has been reported for PDMS−graphene made using a nickel foam template and chemical vapor deposition.[36] This foam is particularly suitable for flexible applications, owing to its very low density.[36] Also, a slightly higher value of 25.7 dB·g^{-1}·cm^3·mm^{-1} has been reported for PS−graphene at a high loading of 30 wt % graphene.[35] However, these composite foams employ nanosized particles that are much more expensive than the SSF fibers used in the current work. Furthermore, all of these foam composites have been fabricated in a batch-type system, which is not easily adaptable to the current manufacturing methods.

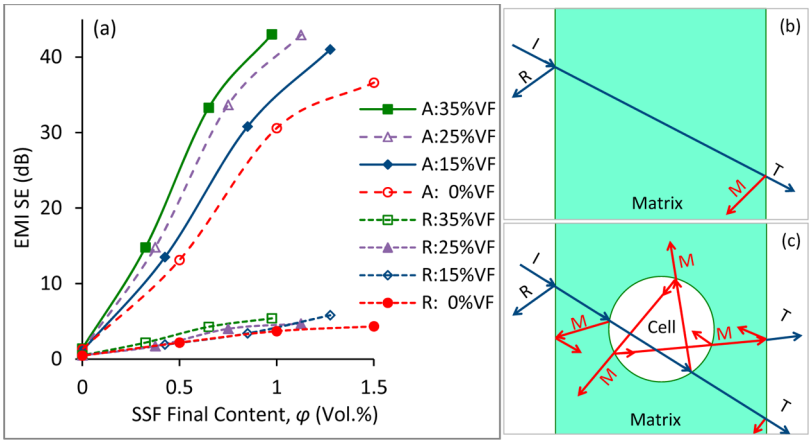

Figure 8. (a) Absorption (A in the legend) and reflection (R in the legend) SE of the injection-molded PP−SSF composites at various void fractions. (b and c) Schematic illustrations of the electromagnetic wave reflection, transmission, and multiple reflection in solid and foam samples, respectively. I, R, T, and M denote the incident, reflected, transmitted, and multiple-reflected waves, respectively.

The PP−SSF composite foams of the current work were fabricated using foam injection molding, which can be readily adapted to the manufacturing of foam shields as substitutes for electronic frames and housing because injection molding is their current manufacturing method.

To further understand the effects of foaming on the EMI shielding performance, the contributions of the absorption and reflection mechanisms to the total SE were also determined following the procedure described in our earlier work[1] and reported in Figure 8. As can be seen, the shielding by reflection was similar in both SIM and FIM composites. This was expected because the surfaces of both solid and foam composites were similar in terms of the local filler content because the foam samples also had a solid skin layer.[1] Shielding by reflection slowly increased with the SSF content, reaching to a maximum of about 5 dB. Therefore, the shielding by absorption, which is desired in most of the applications, was the dominant attenuation mechanism, and it continuously increased with an increase of the SSF content in both SIM and FIM composites. Compared to the SIM samples, the shielding by absorption was higher for the FIM samples and continuously increased as the void fraction was increased from 0 to 35%. The enhanced SE via absorption in the foam composites stemmed from two different mechanisms. Less fiber breakage, a change of the fiber orientation state, and a possible increase in the interconnectivity of the fibers via physical foaming contributed to an increase of the electrical conductivity (Figure 2) and dielectric permittivity[1] and thus resulted in an increased SE.[1,58,62] In addition, multiple reflection, which is the electromagnetic wave reflection at various surfaces and interfaces inside the shield,[63] was another shielding mechanism that was affected by the cellular structure. The existence of cells created a huge gaseous cell−composite matrix surface area inside the shield. The incident electromagnetic waves entering the foam samples were reflected and scattered at the cell−matrix interfaces numerous times. This multiple reflection combined with the adequate level of wave absorption capability inside the composite matrix resulted in the further attenuation of electromagnetic waves and thereby improved the EMI SE in the foam samples.[30,64] The difference between the wave scattering and multiple reflection in the solid and foam samples is schematically presented in Figure 8b,c. It is noted that the shielding by multiple reflection cannot be separately measured and its effect is hidden in the absorption and reflection measurements.

4. SUMMARY

The microstructure, fiber breakage, electrical properties, and EMI SE of the SIM and FIM PP−SSF composites having void fractions as high as 35% were characterized.

Generation of physical foaming altered the microstructure of the PP−SSF composites predominantly through the plasticizing effect of dissolved gas in a polymer melt. The dissolved gas significantly reduced the fiber breakage and attenuated the fiber preferential orientation via viscosity reduction.

The microstructural changes through foaming resulted in a reduction of the density of up to 35% and the enhancement of the electrical and EMI SE performance. The percolation threshold of 0.85 vol % in solid composites continuously decreased with an increase in the void fraction and reached 0.21 vol % at 35% void fraction, accounting for more than a 4-fold decrease. Both the absolute and specific EMI SE values were also increased by foaming. A maximum specific EMI SE of 75 $dB{\cdot}g^{-1}{\cdot}cm^3$ was achieved in PP−1.1 vol % SSF composite foams, which was highly superior to 38 $dB{\cdot}g^{-1}{\cdot}cm^3$ of the solid PP−1.0 vol % SSF composites.

The results obtained in this investigation reveal that lightweight conductive products with a low filler content and enhanced electrical and EMI shielding properties can be developed with the aid of foaming in the injection-molding process for applications in the electronics, aerospace, and automotive industries.

AUTHOR INFORMATION

Corresponding Author

*Tel: 416-978-3053. Fax: 416-978-0947. E-mail: park@mie.utoronto.ca.

Author Contributions

The manuscript was written through contributions of all authors. All authors have given approval to the final version of the manuscript.

Notes

The authors declare no competing financial interest.

■ ACKNOWLEDGMENTS

This work was financially supported by the Natural Science and Engineering Research Council of Canada (Grant DG154279-2010) and the Consortium for Cellular and Microcellular Plastics.

■ REFERENCES

(1) Ameli, A.; Jung, P. U.; Park, C. B. Electrical Properties and Electromagnetic Interference Shielding Effectiveness of Polypropylene/Carbon Fiber Composite Foams. *Carbon* **2013**, 379−391.
(2) Paul, C. R. *Introduction to Electromagnetic Compatibility*, 2nd ed.; John Wiley and Sons Inc.: Hoboken, NJ, 2006.
(3) Lee, H. C.; Kim, J. Y.; Noh, C. H.; Song, K. Y.; Cho, S. H. Selective Metal Pattern Formation and Its EMI Shielding Efficiency. *Appl. Surf. Sci.* **2006**, *252*, 2665−2672.
(4) Schlechter, M. EMI/RFI: Materials and Technology, www.bccresearch.com (accessed Apr 29, 2014).
(5) Sun, X.; Cheng, Y.; Wu, H. Research on Microstructure and Electrical Resistivity of Injection Molded Metallic Fiber-Filled Polymer Composites. *Adv. Mater. Res.* **2012**, *472*, 748−752.
(6) Al-Saleh, M. H.; Sundararaj, U. T. Electromagnetic Interference (EMI) Shielding Effectiveness of PP/PS Polymer Blends Containing High Structure Carbon Black. *Macromol. Mater. Eng.* **2008**, *293*, 621−630.
(7) Jana, P. B.; Mallick, A. K.; De, S. K. Effects of Sample Thickness and Fiber Aspect Ratio on EMI Shielding Effectiveness of Carbon Fiber Filled Polychloroprene Composites in the X-Band Frequency Range. *IEEE Trans. Electromagn. Compat.* **1992**, *34*, 478−481.
(8) Krueger, Q. J.; King, J. A. Synergistic Effects of Carbon Fillers on Shielding Effectiveness in Conductive Nylon 6,6- and Polycarbonate-Based Resins. *Adv. Polym. Technol.* **2003**, *22*, 96−111.
(9) Chang, H.; Kao, M.-J.; Huang, K.-D.; Kuo, C.-G.; Huang, S.-Y. Electromagnetic Shielding Effectiveness of Thin Film with Composite Carbon Nanotubes and Stainless Steel Fibers. *J. Nanosci. Nanotechnol.* **2011**, *11*, 1754−1757.
(10) Das, N. C.; Khastgir, D.; Chaki, T. K.; Chakraborty, A. Electromagnetic Interference Shielding Effectiveness of Carbon Black and Carbon Fiber Filled EVA and NR Based Composites. *Composites, Part A* **2000**, *31*, 1069−1081.
(11) Arjmand, M.; Mahmoodi, M.; Gelves, G. A.; Park, S.; Sundararaj, U. T. Electrical and Electromagnetic Interference Shielding Properties of Flow-Induced Oriented Carbon Nanotubes in Polycarbonate. *Carbon* **2011**, *49*, 3430−3440.
(12) Kim, H. M.; Kim, K.; Lee, C. Y.; Joo, J.; Cho, S. J.; Yoon, H. S.; et al. Electrical Conductivity and Electromagnetic Interference Shielding of Multiwalled Carbon Nanotube Composites Containing Fe Catalyst. *Appl. Phys. Lett.* **2004**, *84*, 589−591.
(13) Yang, Y. L.; Gupta, M. C.; Dudley, K. L.; Lawrence, R. W. Novel Carbon Nanotube−Polystyrene Foam Composites for Electromagnetic Interference Shielding. *Nano Lett.* **2005**, *5*, 2131−2134.
(14) Zhang, C. S.; Ni, Q. Q.; Fu, S. Y.; Kurashiki, K. Electromagnetic Interference Shielding Effect of Nanocomposites with Carbon Nanotube and Shape Memory Polymer. *Compos. Sci. Technol.* **2007**, *67*, 2973−2980.
(15) Li, N.; Huang, Y.; Du, F.; He, X. B.; Lin, X.; Gao, H. J.; et al. Electromagnetic Interference (EMI) Shielding of Single-Walled Carbon Nanotube Epoxy Composites. *Nano Lett.* **2006**, *6*, 1141−1145.
(16) Liu, Z. F.; Bai, G.; Huang, Y.; Ma, Y. F.; Du, F.; Li, F. F.; et al. Reflection and Absorption Contributions to the Electromagnetic Interference Shielding of Single-Walled Carbon Nanotube/Polyurethane Composites. *Carbon* **2007**, *45*, 821−827.
(17) Zhang, G.; Thompson, M. R. Reduced Fibre Breakage in a Glass-Fibre Reinforced Thermoplastic through Foaming. *Compos. Sci. Technol.* **2005**, *65*, 2240−2249.
(18) Arjmand, M.; Mahmoodi, M.; Park, S.; Sundararaj, U. T. An Innovative Method to Reduce the Energy Loss of Conductive Filler/Polymer Composites for Charge Storage Applications. *Compos. Sci. Technol.* **2013**, *78*, 24−29.
(19) Motlagh, G. H.; Hrymak, A. N.; Thompson, M. R. Improved Through-Plane Electrical Conductivity in a Carbon-Filled Thermoplastic via Foaming. *Polym. Eng. Sci.* **2008**, *48*, 687−696.
(20) Ameli, A.; Jung, P. U.; Park, C. B. Through-Plane Electrical Conductivity of Injection-Molded Polypropylene/Carbon-Fiber Composite Foams. *Compos. Sci. Technol.* **2013**, *76*, 37−44.
(21) Antunes, M.; Mudarra, M.; Velasco, J. I. Broadband Electrical Conductivity of Carbon Nanofibre-Reinforced Polypropylene Foams. *Carbon* **2011**, *49*, 708−717.
(22) Shen, B.; Zhai, W.; Lu, D.; Zheng, W.; Yan, Q. Fabrication of Microcellular Polymer/Graphene Nanocomposite Foams. *Polym. Int.* **2012**, *61*, 1693−1702.
(23) Okamoto, M.; Nam, P. H.; Maiti, M.; Kotaka, T.; Nakayama, T.; Takada, M.; et al. Biaxial Flow-Induced Alignment of Silicate Layers in Polypropylene/Clay Nanocomposite Foam. *Nano Lett.* **2001**, *1*, 503−505.
(24) Antunes, M.; Gabriel, G.; Velasco, J. I. Multifunctional Nanocomposite Foams Based on Polypropylene with Carbon Nanofillers. *J. Cell. Plast.* **2013**, *49*, 259−279.
(25) Pegel, S.; Pötschke, P.; Petzold, G.; Alig, I.; Dudkin, S. M.; Lellinger, D. Agglomeration and Network Formation of Multiwalled Carbon Nanotubes in Polycarbonate Melts. *Polymer* **2008**, *49*, 974−984.
(26) Müller, M. T.; Krause, B.; Pötschke, P. A Successful Approach to Disperse MWCNTs in Polyethylene by Melt Mixing Using Polyethylene Glycol as Additive. *Polymer* **2012**, *53*, 3079−3083.
(27) Wang, C.; Ying, S.; Xiao, Z. Preparation of Short Carbon Fiber/Polypropylene Fine-Celled Foams in Supercritical CO_2. *J. Cell. Plast.* **2013**, *49*, 65−82.
(28) Ling, J.; Zhai, W.; Feng, W.; Shen, B.; Zhang, J.; Zheng, W. A Facile Preparation of Lightweight Microcellular Polyetherimide/Graphene Composites Foams for Electromagnetic Interference (EMI) Shielding. *ACS Appl. Mater. Interfaces* **2013**, *5*, 2677−2684.
(29) Shen, B.; Zhai, W.; Tao, M.; Ling, J.; Zheng, W. Lightweight, Multifunctional Polyetherimide/Graphene@Fe_3O_4 Composite Foams for Shielding of Electromagnetic Pollution. *ACS Appl. Mater. Interfaces* **2013**, *5*, 11383−11391.
(30) Zhang, H. B.; Yan, Q.; Zheng, W. G.; He, Z.; Yu, Z. Z. Tough Graphene−Polymer Microcellular Foams for Electromagnetic Interference Shielding. *ACS Appl. Mater. Interfaces* **2011**, *3*, 918−924.
(31) Thomassin, J.-M.; Pagnoulle, C.; Bednarz, L.; Huynen, I.; Jerome, R.; Detrembleur, C. Foams of Polycaprolactone/MWNT Nanocomposites for Efficient EMI Reduction. *J. Mater. Chem.* **2008**, *18*, 792−796.
(32) Eswaraiah, V.; Sankaranarayanan, V.; Ramaprabhu, S. Functionalized Graphene−PVDF Foam Composites for EMI Shielding. *Macromol. Mater. Eng.* **2011**, *296*, 894−898.
(33) Fletcher, A.; Gupta, M. C.; Dudley, K. L.; Vedeler, E. Elastomer Foam Nanocomposites for Electromagnetic Dissipation and Shielding Applications. *Compos. Sci. Technol.* **2010**, *70*, 953−958.
(34) Yang, Y.; Gupta, M. C.; Dudley, K. L.; Lawrence, R. W. Conductive Carbon Nanofiber−Polymer Foam Structures. *Adv. Mater.* **2005**, *17*, 1999−2003.
(35) Yan, D. X.; Ren, P. G.; Pang, H.; Fu, Q.; Yang, M.-B.; Li, Z.-M. Efficient Electromagnetic Interference Shielding of Lightweight Graphene/Polystyrene Composite. *J. Mater. Chem.* **2012**, *22*, 18772−18774.
(36) Chen, Z.; Xu, C.; Ma, C.; Ren, W.; Cheng, H.-M. Lightweight and Flexible Graphene Foam Composites for High-Performance Electromagnetic Interference Shielding. *Adv. Mater.* **2013**, *25*, 1296−1300.
(37) Chen, Z.; Ren, W.; Gao, L.; Liu, B.; Pei, S.; Cheng, H.-M. Three-dimensional Flexible and Conductive Interconnected Graphene Networks Grown by Chemical Vapour Deposition. *Nat. Mater.* **2011**, *10*, 424−428.
(38) Bernal, M. M.; Gallego, M. M.; Molenberg, I.; Huynen, I.; Manchado, M. A. L.; Verdejo, R. Influence of Carbon Nanoparticles on the Polymerization and EMI Shielding Properties of PU Nanocomposite Foams. *RSC Adv.* **2014**, *4*, 7911−7918.

(39) Antunes, M.; Velasco, J. I. Multifunctional Polymer Foams with Carbon Nanoparticles. *Prog. Polym. Sci.* **2014**, *39*, 486−509.
(40) Thomassin, J.-M.; Jerome, C.; Pardoen, T.; Bailly, C.; Huynen, I.; Detrembleur, C. Polymer/Carbon Based Composites as Electromagnetic Interference (EMI) Shielding. *Mater. Sci. Eng., R* **2013**, *74*, 211−232.
(41) Ameli, A.; Nofar, M.; Park, C. B.; Pötschke, P.; Rizvi, G. Polypropylene/Carbon Nanotube Nano/Microcellular Structures with High Dielectric Permittivity, Low Dielectric Loss, and Low Percolation Threshold. *Carbon* **2014**, *71*, 206−217.
(42) Li, G.; Gunkel, F.; Wang, J.; Park, C. B.; Altstädt, V. Solubility Measurements of N_2 and CO_2 in Polypropylene and Ethene/Octene Copolymer. *J. Appl. Polym. Sci.* **2007**, *103*, 2945−2953.
(43) Li, G.; Wang, J.; Park, C. B.; Simha, R. Measurement of Gas Solubility in Linear/Branched PP Melts. *J. Polym. Sci., B: Polym. Phys.* **2007**, *45*, 2497−2508.
(44) Lee, J. W. S.; Wang, J.; Yoon, J. D.; Park, C. B. Strategies to Achieve a Uniform Cell Structure with a High Void Fraction in Advanced Structural Foam Molding. *Ind. Eng. Chem. Res.* **2008**, *47*, 9457−9464.
(45) Ameli, A.; Jahani, D.; Nofar, M.; Jung, P. U.; Park, C. B. Processing and Characterization of Solid and Foamed Injection-Molded Polylactide with Talc. *J. Cell. Plast.* **2013**, *49*, 351−374.
(46) Ameli, A.; Jahani, D.; Nofar, M.; Jung, P. U.; Park, C. B. Development of High Void Fraction Polylactide Composite Foams Using Injection Molding: Mechanical and Thermal Insulation Properties. *Compos. Sci. Technol.* **2014**, *90*, 88−95.
(47) Ameli, A.; Nofar, M.; Jahani, D.; Park, C. B. Development of High Void Fraction Polylactide Composite Foams Using Injection Molding: Crystallization and Foaming Behaviors. *Chem. Eng. J.* submitted **2014**, CEJ-D-14-00115.
(48) Kirkpatrick, S. Percolation and Conduction. *Rev. Mod. Phys.* **1973**, *45*, 574−588.
(49) Weber, M.; Kamal, M. R. Estimation of the Volume Resistivity of Electrically Conductive Composites. *Polym. Compos.* **1997**, *18*, 726−740.
(50) Dani, A.; Ogale, A. A. Electrical Percolation Behavior of Short Fiber Composites: Experimental Characterization and Modeling. *Compos. Sci. Technol.* **1996**, *56*, 911−920.
(51) Yi, J. Y.; Choi, G. M. Percolation Behavior of Conductor−Insulator Composites with Varying Aspect Ratio of Conductive Fiber. *J. Electroceram.* **1999**, *3*, 361−369.
(52) Taipalus, R.; Harmia, T.; Zhang, M. Q.; Friedrich, K. The Electrical Conductivity of Carbon-Fibre-Reinforced Polypropylene/Polyaniline Complex-Blends: Experimental Characterisation and Modeling. *Compos. Sci. Technol.* **2001**, *61*, 801−814.
(53) Foulger, S. H. Reduced Percolation Thresholds of Immiscible Conductive Blends. *Polym. Sci.: Polym. Phys.* **1999**, *37*, 1899−1910.
(54) Al-Saleh, M. H.; Sundararaj, U. T. Microstructure, Electrical, and Electromagnetic Interference Shielding Properties of Carbon Nanotube/Acrylonitrile−Butadiene−Styrene Nanocomposites. *Polym. Sci.: Polym. Phys.* **2012**, *50*, 1356−1362.
(55) Logakis, E.; Pandis, C.; Pissis, P.; Pionteck, J.; Pötschke, P. Highly Conducting Poly(Methyl Methacrylate)/Carbon Nanotubes Composites: Investigation on their Thermal, Dynamic-Mechanical, Electrical and Dielectric Properties. *Compos. Sci. Technol.* **2011**, *71*, 854−862.
(56) McNally, T.; Pötschke, P.; Halley, P.; Murphy, M.; Martin, D.; Bell, S. E. J.; et al. Polyethylene Multiwalled Carbon Nanotube Composites. *Polymer* **2005**, *46*, 8222−8232.
(57) Meincke, O.; Kaempfer, D.; Weickmann, H.; Friedrich, C.; Vathauer, M.; Warth, H. Mechanical Properties and Electrical Conductivity of Carbon- Nanotube Filled Polyamide-6 and Its Blends with Acrylonitrile/Butadiene/Styrene. *Polymer* **2004**, *45*, 739−748.
(58) Al-Saleh, M. H.; Gelves, G. A.; Sundararaj, U. T. Copper Nanowire/Polystyrene Nanocomposites: Lower Percolation Threshold and Higher EMI Shielding. *Composites, Part A* **2011**, *42*, 92−97.
(59) Shui, X. P.; Chung, D. D. L. Nickel Filament Polymer−Matrix Composites with Low Surface Impedance and High Electromagnetic Interference Shielding Effectiveness. *J. Electron. Mater.* **1997**, *26*, 928−934.
(60) Li, L.; Chung, D. D. L. Electrical and Mechanical Properties of Electrically Conductive Polyethersulfone Composite. *Composites* **1994**, *25*, 215−224.
(61) Li, L.; Chung, D. D. L. Effect of Viscosity on the Electrical Properties of Conducting Thermoplastic Composites Made by Compression Molding of a Powder Mixture. *Polym. Compos.* **1993**, *14*, 467−472.
(62) Mahmoodi, M.; Arjmand, M.; Sundararaj, U. T.; Park, S. The Electrical Conductivity and Electromagnetic Interference Shielding of Injection Moulded Multi-walled Carbon Nanotube/polystyrene Composites. *Carbon* **2012**, *50*, 1455−1464.
(63) Al-Saleh, M. H.; Sundararaj, U. T. Electromagnetic Interference Shielding Mechanisms of CNT/Polymer Composites. *Carbon* **2009**, *47*, 1738−1746.
(64) Wang, J. C.; Xiang, C. S.; Liu, Q.; Pan, Y. B.; Guo, J. K. Ordered Mesoporous Carbon/Fused Silica Composites. *Adv. Funct. Mater.* **2008**, *18*, 2995−3002.